HHS Public Access

Author manuscript

Eur J Appl Physiol. Author manuscript; available in PMC 2017 January 01.

Published in final edited form as:

Eur J Appl Physiol. 2016 January ; 116(1): 97–113. doi:10.1007/s00421-015-3228-3.

Simple Accurate Mathematical Models of Blood HbO_2 and $HbCO_2$ Dissociation Curves at Varied Physiological Conditions– Evaluation and Comparison with other Models

Ranjan K. Dash, Ph.D.,

Department of Physiology, Biotechnology and Bioengineering Center, Medical College of Wisconsin, 8701 Watertown Plank Road, Milwaukee, WI-53226, Phone: 414-955-4497

Ben Korman, M.B.B.S., M.D., and

Department of Anaesthesia and Pain Medicine, Royal Perth Hospital, Perth, Western Australia, Australia

James B. Bassingthwaighte, M.D., Ph.D.

Department of Bioengineering, Box 355061, N210G North Foege Bldg., University of Washington, Seattle, WA 9895-5061, USA, Phone: 206-685-2012

Ranjan K. Dash: rdash@mcw.edu; Ben Korman: ben@korman.com.au; James B. Bassingthwaighte: jbb2@u.washington.edu

Abstract

Purpose—Equations for blood oxyhemoglobin (HbO_2) and carbaminohemoglobin ($HbCO_2$) dissociation curves that incorporate nonlinear biochemical interactions of oxygen and carbon dioxide with hemoglobin (Hb), covering a wide range of physiological conditions, are crucial for a number of practical applications. These include the development of physiologically-based computational models of alveolar-blood and blood-tissue O_2-CO_2 transport, exchange, and metabolism, and the analysis of clinical and in-vitro data.

Method and Results—To this end, we have revisited, simplified, and extended our previous models of blood HbO_2 and $HbCO_2$ dissociation curves (Dash and Bassingthwaighte, Ann. Biomed. Eng. 38:1683–1701, 2010), validated wherever possible by available experimental data, so that the models now accurately fit the low HbO_2 saturation (S_{HbO2}) range over a wide range of values of P_{O2}, P_{CO2}, pH, 2,3-DPG, and temperature. Our new equations incorporate a novel P_{O2}-dependent variable cooperativity hypothesis for the binding of O_2 to Hb, and a new equation for P_{50} of O_2 that provides accurate shifts in the HbO_2 and $HbCO_2$ dissociation curves over a wide range of physiological conditions. The accuracy and efficiency of these equations in computing P_{O2} and P_{CO2} from the S_{HbO2} and S_{HbCO2} levels using simple iterative numerical schemes that give rapid convergence is a significant advantage over alternative S_{HbO2} and S_{HbCO2} models.

Conclusion—The new S_{HbO2} and S_{HbCO2} models have significant computational modeling implications as they provide high accuracy under non-physiological conditions, such as ischemia and reperfusion, extremes in gas concentrations, high altitudes, and extreme temperatures.

Correspondence to: Ranjan K. Dash, rdash@mcw.edu; James B. Bassingthwaighte, jbb2@u.washington.edu.

Keywords

O_2 and CO_2 binding to hemoglobin; O_2 and CO_2 saturation of hemoglobin; Oxyhemoglobin and carbaminohemoglobin dissociation curves; Nonlinear O_2-CO_2 interactions; Bohr and Haldane effects; Mathematical modeling

Introduction

The delivery of oxygen to tissues for metabolism and energy production in parenchymal cells is regulated by a complex system of physicochemical processes in the microcirculation (Dash & Bassingthwaighte, 2006; Bassingthwaighte *et al.*, 2012). In systemic capillaries, the release of oxygen from hemoglobin (Hb) inside red blood cells (RBCs) depends in part on the simultaneous release of carbon dioxide into the flowing blood. In the lungs, the loss of CO_2 from RBCs increases O_2 uptake, which in turn enhances CO_2 dissociation from Hb. This interacting process also depends on the buffering of CO_2 by bicarbonate ions (HCO_3^-), acid-base regulation, and the Hb-mediated nonlinear biochemical O_2-CO_2 interactions inside RBCs (Geers & Gros, 2000; Rees & Andreassen, 2005; Dash & Bassingthwaighte, 2006; Bassingthwaighte *et al.*, 2012). In this regard, a decrease in pH or an increase in CO_2 partial pressure (P_{CO2}) in systemic capillaries decreases the affinity of O_2 for Hb and HbO_2 saturation (S_{HbO2}), and increases the delivery of O_2 to peripheral tissues (the Bohr effect). On the other hand, an increase in O_2 partial pressure (P_{O2}) in pulmonary capillaries results in the release of hydrogen ions (H^+) from Hb, which in turn decreases the affinity of Hb for CO_2, reducing $HbCO_2$ saturation (S_{HbCO2}) and aiding elimination of CO_2 by the lungs (the Haldane effect). Thus, both the Bohr and Haldane effects are important in defining the Hb-mediated nonlinear biochemical O_2-CO_2 interactions inside RBCs (Siggaard-Andersen & Garby, 1973; Tyuma, 1984; Matejak *et al.*, 2015). Raising blood temperature (T) also lowers the affinity of O_2 for Hb, and increases the delivery of O_2 to tissues. Consequently, the integrated computational modeling of O_2 transport, exchange and metabolism in tissue-organ systems must account for the coupled transport and exchange of CO_2, HCO_3^-, H^+, and heat in the microcirculation (Dash & Bassingthwaighte, 2006). This is particularly important in highly metabolic tissue-organ systems such as heart and skeletal muscle during exercise (von Restorff *et al.*, 1977), where arterio-venous (AV) temperature increases of 1 °C or so, P_{CO2} increases of nearly 10 mmHg, and pH decreases of about 0.1 pH unit, all combine to push the HbO_2 dissociation curve to the right. Under these conditions, P_{O2} may decrease by as much as 80 mmHg and S_{HbO2} may decrease to less than 10% along capillaries which may be shorter than one millimetre in length. To properly account for the mass balance throughout the capillary-tissue exchange region, it is necessary to compute the changes associated with the nonlinear biochemical O_2-CO_2 interactions in blood as influenced by P_{O2}, P_{CO2}, pH, and T, thus the need for accurate and efficient forward and invertible S_{HbO2} and S_{HbCO2} equations.

In order to quantify the Bohr and Haldane effects as well as the synergistic effects of 2,3-DPG and T, Dash and Bassingthwaighte (2004; 2010) have developed new mathematical models of O_2 and CO_2 saturation of Hb (S_{HbO2} and S_{HbCO2}) based on equilibrium binding of O_2 and CO_2 to Hb inside RBCs. They are in the form of an invertible Hill-type equation

with apparent binding constants K_{HbO2} and K_{HbCO2} which depend on the levels of P_{O2}, P_{CO2}, pH, 2,3-DPG, and T in blood. The invertibility of these new equations enables analytical calculations of P_{O2} from S_{HbO2} and P_{CO2} from S_{HbCO2} and vice-versa. This is especially important for the integrated computational modeling of simultaneous transport and exchange of O_2 and CO_2 in alveolar-blood and blood-tissue exchange systems (Dash & Bassingthwaighte, 2006). The HbO_2 dissociation curves computed from the S_{HbO2} model are in very good agreement with previously published experimental and theoretical curves in the literature over a wide range of physiological conditions (Kelman, 1966b; Severinghaus, 1979; Winslow *et al.*, 1983; Siggaard-Andersen *et al.*, 1984; Buerk & Bridges, 1986). However, as with any theoretical model, there are some limitations in the 2010 Dash and Bassingthwaighte S_{HbO2} and S_{HbCO2} models. In particular, the S_{HbO2} model is only accurate for values of S_{HbO2} lying between 0.3 and 0.98 (with a Hill coefficient nH of 2.7), even if accounting well in that range for the effects of pH, P_{CO2}, 2,3-DPG and T. Furthermore, the S_{HbO2} and S_{HbCO2} models require complicated calculations of the indices n_1, n_2, n_3, and n_4 involved in the expression for the apparent equilibrium constant in a single-step O_2-Hb binding reaction (Dash & Bassingthwaighte, 2010). These limitations are addressed here by simplifying the S_{HbO2} and S_{HbCO2} models further and extending the accuracy of the S_{HbO2} model to the whole S_{HbO2} range for the varied physiological conditions. The resulting S_{HbO2} and S_{HbCO2} models are also tested using diverse experimental data available in the literature on the HbO_2 and $HbCO_2$ dissociation curves for a wide range of physiological conditions (Joels & Pugh, 1958; Naeraa *et al.*, 1963; Bauer & Schroder, 1972; Hlastala *et al.*, 1977; Matthew *et al.*, 1977; Reeves, 1980). This study does not include the buffering of CO_2 in blood as that is covered in our previous work on blood-tissue gas exchange (Dash & Bassingthwaighte, 2006) and by Wolf (2013) for whole-body acid-base and electrolyte balance. Interested readers are referred to our previous article (Dash & Bassingthwaighte, 2010) for a historical perspective and details of the mathematical models of S_{HbO2} not covered in this paper.

Methods

Simple Mathematical Expressions for S_{HbO2} and S_{HbCO2}

Based on the detailed nonlinear biochemical interactions of O_2 and CO_2 with Hb inside RBCs, Dash and Bassingthwaighte (2010) derived the following mechanistic mathematical expressions for the fractional saturation of Hb with O_2 and CO_2 (S_{HbO2} and S_{HbCO2}, respectively):

$$S_{HbO2}=\frac{K_{HbO2}[O_2]}{1+K_{HbO2}[O_2]};\quad S_{HbCO2}=\frac{K_{HbCO2}[CO_2]}{1+K_{HbCO2}[CO_2]} \quad (1a,b)$$

Here the concentrations are in moles per liter or M with respect to the water space of RBCs. The concentration of free O_2 or free CO_2 in the water space of RBCs may also be expressed in terms of the partial pressure of O_2 or CO_2 so that $[O_2] = \alpha_{O2}P_{O2}$ and $[CO_2] = \alpha_{CO2}P_{CO2}$, where α_{O2} and α_{CO2} are the solubilities of O_2 and CO_2 in water, computed from their measured values in plasma (Austin *et al.*, 1963; Hedley-Whyte & Laver, 1964) and

corrected for the effects of temperature (Kelman, 1966a; 1967; Dash & Bassingthwaighte, 2010):

$$\alpha_{O2}=\left[1.37-1.37\times10^{-2}(T-37)+5.8\times10^{-4}(T-37)^2\right]\left[10^{-6}/W_{pl}\right]\ \mathrm{M/mmHg} \quad (2a)$$

$$\alpha_{CO2}=\left[3.07-5.7\times10^{-2}(T-37)+2\times10^{-3}(T-37)^2\right]\left[10^{-5}/W_{pl}\right]\ \mathrm{M/mmHg} \quad (2b)$$

Here W_{pl} = 0.94 is the fractional water space of plasma and T is in degrees centigrade (°C). Thus =α_{O2}1.46×10^{-6} M/mmHg and α_{CO2} = 3.27×10^{-5} M/mmHg at 37 °C (see Table 1). The expressions for [O_2] and [CO_2] in terms of P_{O2} and P_{CO2} and vice-versa are freely interchanged throughout this paper. The apparent equilibrium constants of Hb with O_2 and CO_2 (K_{HbO2} and K_{HbCO2} with units of M^{-1}), based on single-step bindings of O_2 and CO_2 to Hb, are reproduced here from Dash and Bassingthwaighte (2010) in a simplified form, introducing the new variables Φ_1 − Φ_4:

$$K_{HbO2}=\frac{K_4'(K_3'[CO_2]\Phi_2+\Phi_4)}{K_2'[CO_2]\Phi_1+\Phi_3};\quad K_{HbCO_2}=\frac{K_2'\Phi_1+K_3'K_4'[O_2]\Phi_2}{\Phi_3+K_4'[O_2]\Phi_4} \quad (3a,b)$$

where the molar concentrations of the gases O_2 and CO_2 are used; the terms Φ_1 − Φ_4 involving the interactions of H^+ with Hb-bound O_2 and CO_2 are given by:

$$\Phi_1=1+\frac{K_2''}{[H^+]};\quad \Phi_2=1+\frac{K_3''}{[H^+]};\quad \Phi_3=1+\frac{[H^+]}{K_5''};\quad \Phi_4=1+\frac{[H^+]}{K_6''} \quad (4a–d)$$

Here [H^+] = 10^{-pH} in RBCs. Given the pH of plasma, the pH of RBCs can be obtained using the simple relationship established by Siggaard-Andersen and colleagues (Siggaard-Andersen, 1971; Siggaard-Andersen & Salling, 1971): pH_{rbc} = 0.795pH_{pl} + 1.357, giving the Gibbs-Donnan ratio for electrochemical equilibrium of H^+ and HCO_3^- across the RBC membrane as a function of pH_{pl}: R_{rbc} = 10$^{-(pH_{pl}-pH_{rbc})}$ = 10$^{-(0.205pH_{pl}-1.357)}$ (see Table 1). In our previous S_{HbO2} and S_{HbCO2} models (Dash & Bassingthwaighte, 2010), R_{rbc} was considered as a constant: R_{rbc} = 0.69, a value corresponding to pH_{pl} = 7.4 and pH_{rbc} = 7.24 (see Table 1).

With these relationships (Eqs. 1–4), the total O_2 and CO_2 concentrations in whole blood can be calculated, as described in the Appendix of the Dash and Bassingthwaighte (2010) paper (see Table 1), and hence are not covered here in detail.

Dependency of K_4' on the Physiological Variables of Interest

Except for K_4', the binding association/dissociation constants are all specified in Table 1. K_4' represents the single-step binding association constant of O_2 with each heme chain of Hb ($HmNH_2$) according to the following hypothetical reaction scheme (Dash & Bassingthwaighte, 2010):

$$O_2 + HmNH_2 \overset{K_4'}{\rightleftharpoons} O_2HmNH_2 \quad (5)$$

The fundamental S-shape of the HbO_2 dissociation curve results from the form of Eq. 1a and the values taken by the product K_{HbO2} $[O_2]$, which depends on K_4'. For any given range of $[O_2]$, the shifts in the HbO_2 dissociation curve with respect to varying physiological conditions arise from the dependence of K_{HbO2} on $[CO_2]$, $[H^+]$ (via Φ_1–Φ_4), and K_4'. Similarly, the shape of the $HbCO_2$ dissociation curve results from the form of Eq. 1b and the values taken by the product K_{HbCO2} $[CO_2]$, which also depends on K_4'. For any given range of $[CO_2]$, the shifts in the $HbCO_2$ dissociation curve with respect to varying physiological conditions arise from the dependence of K_{HbCO2} on $[O_2]$, $[H^+]$ (via Φ_1–Φ_4), and K_4'. From the above description, it is clear that determining K_4' is a critical step in the application of Eqs. 1a and 1b. In our previous S_{HbO2} and S_{HbCO2} models (Dash & Bassingthwaighte, 2010), K_4' is expressed as a complicated function of $[O_2]$, $[CO_2]$, $[H^+]$, [DPG] and T involving the exponents n_0, n_1, n_2, n_3 and n_4, which, except for n_0 (a constant equal to 1.7), are themselves complicated functions of these physiological variables and P_{50} of O_2. In the section below, we show how a very simple expression for K_4' can be obtained without involving the exponents n_0–n_4, significantly simplifying the S_{HbO2} and S_{HbCO2} models.

Derivation of Simple Mathematical Expression for K_4'

Hill's exponent model for S_{HbO2} is based on an n^{th}-order one-step binding of Hb with O_2:

$$S_{HbO2} = \frac{(P_{O2}/P_{50})^n}{1+(P_{O2}/P_{50})^n} \quad (6)$$

Here $n = nH$, the Hill coefficient, is approximately 2.7 for normal human blood; P_{50} is the value of P_{O2} at which Hb is 50 percent saturated by O_2. In Eq. 6, the shifts of the HbO_2 dissociation curve produced by varying physiological conditions arise because P_{50} is a function of P_{CO2}, pH, [DPG] and T, as described below. If Eq. 1a and Eq. 6 are to give identical HbO_2 dissociation curves, we must have $K_{HbO2}\ \alpha_{O2}P_{O2} = (P_{O2}/P_{50})^{nH}$, which when simplified gives:

$$K_4' = \frac{(\alpha_{O2}P_{O2})^{nH-1}\left(K_2'\alpha_{CO2}P_{CO2}\Phi_1+\Phi_3\right)}{(\alpha_{O2}P_{50})^{nH}\left(K_3'\alpha_{CO2}P_{CO2}\Phi_2+\Phi_4\right)} \quad (7)$$

While it is simple to compute S_{HbO2} from Eq. 6, this is not true for S_{HbCO2}. However, Eq. 7 provides an expression for K_4' in terms of P_{O2}, P_{CO2}, pH and P_{50}, which along with Eq. 1b and Eq. 3b describes a simplified model for the $HbCO_2$ dissociation curve. Note also that Eq. 7 can be written in the following alternative form:

$$K_4' = \left(\frac{1}{\alpha_{O2} P_{O2}}\right)\left(\frac{S_{HbO_2}}{1-S_{HbO_2}}\right)\left(\frac{K_2'\alpha_{CO2}P_{CO2}\Phi_1+\Phi_3}{K_3'\alpha_{CO2}P_{CO2}\Phi_2+\Phi_4}\right) \quad (8)$$

so that as S_{HbO2} approaches 1, K_4' becomes infinitely large and K_{HbCO2} becomes equal to $K_3'\Phi_2/\Phi_4$ in Eq. 3b. If a "Division by Zero" error is to be avoided when calculating K_{HbCO2} in computer programs based on these equations, it is necessary to identify situations in which S_{HbO2} might equal 1 (at very high P_{O2}), bypass Eq. 7, and immediately set $K_3'\Phi_2/\Phi_4$.

Simple Mathematical Expression for P_{50} of O_2

P_{50} is a function of P_{CO2}, pH, [DPG] and T. Dash and Bassingthwaighte (2010) obtained a polynomial expression for P_{50} by varying one of these variables at a time, while keeping the other three fixed at their standard physiological values. The resulting polynomial expressions for $P_{50,\Delta pH}$, $P_{50,\Delta CO2}$, $P_{50,\Delta DPG}$, and $P_{50,\Delta T}$ were fitted to the reported P_{50} data from the studies of Buerk and Bridges (1986) and Winslow et al. (1983). These polynomial expressions from Dash and Bassingthwaighte (2010) are further refined here based on additional experimental data from Joels and Pugh (1958), Naeraa et al. (1963), Hlastala et al. (1977), and Reeves (Reeves, 1980) that provide appropriate shifts in S_{HbO2} with varying pH, P_{CO2} and T:

$$P_{50,\Delta pH} = P_{50,S} - 25.535(pH - pH_S) + 10.646(pH - pH_S)^2 - 1.764(pH - pH_S)^3 \quad (9a)$$

$$P_{50,\Delta CO2} = P_{50,S} + 1.273\times10^{-1}(P_{CO2} - P_{CO2,S}) + 1.083\times10^{-4}(P_{CO2} - P_{CO2,S})^2 \quad (9b)$$

$$P_{50,\Delta_{DPG}} = P_{50,S} + 795.63([DPG] - [DPG]_S) - 19660.89([DPG] - [DPG]_S)^2 \quad (9c)$$

$$P_{50,\Delta T} = P_{50,S} + 1.435(T - T_S) + 4.163\times10^{-2}(T - T_S)^2 + 6.86\times10^{-4}(T - T_S)^3 \quad (9d)$$

Here the standard physiological values are denoted by the subscript "S" and are listed in Table 1. The accuracy of the expression for $P_{50,\Delta pH}$ at extreme pH levels has been further improved in Eq. 9a by incorporating the cubic term. Previous researchers (Kelman, 1966b; Severinghaus, 1979; Siggaard-Andersen *et al.*, 1984; Buerk & Bridges, 1986) have shown that for the calculation of P_{50} to be valid when multiple physiological variables are allowed to vary simultaneously, the contribution of each physiological variable to the resulting P_{50} is by multiplication of normalized individual P_{50}'s. Consequently, the expression for P_{50} that best describes the simultaneous varying physiological conditions is given by:

$$P_{50} = P_{50,S}(P_{50,\Delta H}/P_{50,S})(P_{50,\Delta CO2}/P_{50,S})(P_{50,\Delta DPG}/P_{50,S})(P_{50,\Delta T}/P_{50,S}) \quad (10)$$

Incorporation of the Variable Cooperativity Hypothesis

In our previous S_{HbO2} and S_{HbCO2} models (Dash & Bassingthwaighte, 2010), the Hill coefficient *nH* was fixed at 2.7 (or n_0 was fixed at 1.7), making the S_{HbO2} accurate only between 30% and 98%. Next, we extend the accuracy of the modified S_{HbO2} model for the whole saturation range by incorporating an empirical P_{O2}-dependent variable cooperativity hypothesis for O_2 binding to Hb. Specifically, this is achieved by expressing the Hill coefficient *nH* at low P_{O2} as a simple exponential function of P_{O2}:

$$nH = \alpha - \beta \times 10^{-(P_{O2}/\gamma)} \quad (11)$$

where α, β and γ are parameters that govern an apparent cooperativity of O_2 for Hb. Eq. 11 suggests that at low P_{O2}, *nH* is close to $\alpha-\beta$, but increases exponentially towards α with the rate γ as P_{O2} increases. These three parameters along with $P_{50,S}$ are estimated here based on fittings of the S_{HbO2} model to the available experimental data of Severinghaus and colleagues (Roughton *et al.*, 1972; Roughton & Severinghaus, 1973; Severinghaus, 1979) and Winslow et al. (1977) on normal human blood HbO_2 dissociation curves at standard physiological conditions. With *nH* accurately defined by Eq. 11, suitable shifts in the HbO_2 and $HbCO_2$ dissociation curves are achieved through our new expressions for (Eqs. 9 and 10) and K_4' (Eq. 7).

Efficient Numerical Inversion of the S_{HbO2} and S_{HbCO2} Expressions for Practical Usage

Eq. 1a for HbO_2 saturation (S_{HbO2}) is not convenient for analytical inversion, because the apparent equilibrium constant K_{HbO2} for the binding of O_2 to Hb depends on K_4', which in turn depends on P_{O2} (see Eq. 7). However, since Eq. 1a is equivalent to Eq. 6, which depends on P_{50}, which in turn is independent of P_{O2} and is only a function of pH, P_{CO2}, [DPG] and *T*, Eq. 6 can be analytically inverted to compute P_{O2} from S_{HbO2}, subject to the condition that the Hill coefficient *nH* is a constant. When *nH* is allowed to vary with P_{O2}, Eq. 6 can no longer be inverted analytically. However, numerical inversion is possible using efficient iterative schemes such as those presented in the Appendix to this paper. These converge within 8 or less iterations when appropriate starting values are used for P_{O2}. The same approach holds for the inversion of Eq. 1b in the computation of P_{CO2} from S_{HbCO2} (see Appendix), which may not be important clinically, but is of relevance in the integrated computational modeling of simultaneous transport and exchange of respiratory gases in physiological systems. Two efficient numerical methods are presented in the Appendix for the inversion of each gas, based on fixed-point and quasi-Newton-Raphson iteration methods. Similar iterative methods can be used to compute P_{O2} and P_{CO2} from the total $[O_2]$ and the total $[CO_2]$, respectively (these last two parameters are defined in Table 1).

Results

The effect of varying the Hill coefficient *nH* as a function of P_{O2} on the modified S_{HbO2} model simulations at standard physiological conditions is demonstrated through Fig. 1, in which Figs. 1(A,C,E) are based on the data of Severinghaus and colleagues (Roughton *et al.*, 1972; Roughton & Severinghaus, 1973; Severinghaus, 1979), while Figs. 1(B,D,F) are based on the data of Winslow et al. (1977). The first diagram in each set shows how the old and

new S_{HbO2} models (constant and variable *nH*) fit the data in the P_{O2} range of 0–150 mmHg. The inset in each of these two figures shows the fit in the lower P_{O2} range of 0–30 mmHg. It is immediately apparent that the previous S_{HbO2} model, which does not incorporate the variable cooperativity hypothesis, produces a poor fit in the lower 40% saturation range. In Figs. 1(C,D), the residual error in the computed S_{HbO2} relative to the experimental S_{HbO2} is shown for each model for the range of values taken by S_{HbO2}. When the saturation is less than 40%, the residual error is much improved for the new S_{HbO2} model (<0.05% for variable *nH* compared to ~3–% for constant *nH*), and the average residual error over the whole saturation range is virtually zero. Figs. 1(E,F) show how this improvement has been achieved by varying the Hill coefficient *nH* in the low P_{O2} range through the application of Eq. 11 (solid line), compared with the constant value used for *nH* in the old S_{HbO2} model (dashed line). We note here that the *nH* rate parameter γ is related to the $P_{50,S}$ value, which differs slightly for the two different data sets (26.8 mmHg vs. 29.1 mmHg). To achieve the best fit, the parameters α and β also differ slightly between the two different sets of data. This improved accuracy in S_{HbO2} at low P_{O2} may not be relevant clinically, but is important for the computational modeling and mechanistic understanding of *in-vitro* and *in vivo* blood gas data under non-physiological conditions, such as ischemia and reperfusion, extremes in gas concentrations, high altitudes, and extreme temperatures.

The P_{50} values computed from Eqs. 9 and 10 under varying physiological conditions are plotted in Figs. 2(A–D) and are compared to those computed from alternative models from the literature (Kelman, 1967; Buerk & Bridges, 1986; Dash & Bassingthwaighte, 2010). The alternative models do not include corrections based on the experimental data of Joels and Pugh (1958), Naeraa et al. (1963), Hlastala et al. (1977) and Reeves (1980); so for the purpose of this comparison, these corrections have been omitted from Eqs. 9(a–d) by applying appropriate scaling factors of 0.833, 0.588 and 1.02 for $P_{50,\Delta pH}$, $P_{50,\Delta CO2}$ and $P_{50,\Delta T}$, respectively. These simulations show that our scaled P_{50} values agree well with those computed from the model of Buerk and Bridges (1986), that are based on the studies of Winslow et al. (1983). However, they do differ from the P_{50} values computed from the model of Kelman (1966b), where it fails to fit the data at low pH and at either very low or very high P_{CO2}. Our scaled P_{50} values are also improved from our old P_{50} values for pH > 8.5 with the incorporation of the cubic term in Eq. 9a. In addition, the inclusion of corrections based on the diverse experimental data sets of Joels and Pugh (1958), Naeraa et al. (1963), Hlastala et al. (1977), and Reeves (1980) in Eqs. 9(a–d) provides further improvement in the P_{50} values over a wide range of variation in the relevant physiological variables (see description below for Fig. 3). A new model recently published by Mateják et al. (2015), while this article was under preparation, also fits some of these experimental data well under altered physiological conditions. Their approach, a modification of Adair's four-step algorithm (Adair, 1925), considers the problems in depth, and, like ours, relates the O_2-Hb and CO_2-Hb binding effects to the acid-base chemistry of blood based on pH and P_{CO2}, as proposed by Siggaard-Andersen and others over the years (Rossi-Bernardi & Roughton, 1967; Forster *et al.*, 1968; Siggaard-Andersen, 1971; Siggaard-Andersen & Salling, 1971; Bauer & Schroder, 1972; Siggaard-Andersen *et al.*, 1972a; Siggaard-Andersen *et al.*, 1972b; Siggaard-Andersen & Garby, 1973; Siggaard-Andersen *et al.*, 1984; Siggaard-Andersen & Siggaard-Andersen, 1990). Specifically, they effectively express the four Adair coefficients

in terms of the physiological variables of interest (i.e. pH, P_{CO2}, and T they do not consider the effects of 2,3-DPG), providing appropriate shifts in the HbO_2 dissociation curve with altered physiological conditions.

The accuracy and robustness of our simplified and extended models of S_{HbO2} and S_{HbCO2} under varying physiological conditions (P_{50} defined by Eqs. 9 and 10, and variable *nH* defined by Eq. 11) has also been tested against diverse experimental data available from the literature (Joels & Pugh, 1958; Naeraa *et al.*, 1963; Bauer & Schroder, 1972; Hlastala *et al.*, 1977; Matthew *et al.*, 1977; Reeves, 1980), and is illustrated in Fig. 3. Our refined S_{HbO2} model (i.e. the simplified S_{HbO2} model with variable *nH*) is able to reproduce the S_{HbO2} data of Joels and Pugh (1958) and Naeraa et al. (1963) obtained for a range of values of pH and P_{CO2} at 37 °C (Figs. 3A and 3B) as well as the S_{HbO2} data of Hlastala et al. (1977) and Reeves (1980) obtained over a range of values of T at fixed P_{CO2} and pH (Figs. 3C and 3D). These data allow a more accurate determination of the coefficients for use in the polynomial expressions for $P_{50,\Delta pH}$, $P_{50,\Delta CO2}$, $P_{50,\Delta DPG}$, and $P_{50,\Delta T}$, and hence characterize the dependence of P_{50} on pH, P_{CO2}, [DPG] and T, and the corresponding shifts in the HbO_2 dissociation curves. Similarly, our refined model of S_{HbCO2} is able to reproduce the S_{HbCO2} data of Bauer and Schröder (1972) and Matthew et al. (1977) obtained as a function of pH_{rbc} in oxygenated and deoxygenated blood with either constant P_{CO2} of 40 mmHg at 37°C (Fig. 3E) or constant total [CO_2] of 55 mM at 30 °C (Fig. 3F). These model fittings provide accurate estimates of the equilibrium constants associated with the binding of CO_2 to oxygenated and deoxygenated Hb as well as the ionization constants of oxygenated and deoxygenated Hb at 30 °C and 37 °C (see Table 1). These estimates differ slightly from those used in our previous models of S_{HbO2} and S_{HbCO2} (Dash & Bassingthwaighte, 2010), but are in close agreement with those reported by Bauer and Schröder (1972) and Rossi-Bernardi and Roughton (1967). It can be noted here that the estimates of the parameters associated with the P_{O2}-dependent variable *nH* for these different data sets are all similar, further signifying the importance of the variable cooperativity hypothesis in accurately simulating HbO_2 dissociation curves in the whole saturation range under varying physiological conditions.

Simulations of the apparent HbO_2 binding constant K_4', HbO_2 dissociation curves, and $HbCO_2$ dissociation curves over a wide range of physiological conditions (P_{O2}, P_{CO2}, pH, [DPG], and T) are based on our refined models of K_4', S_{HbO2} and S_{HbCO2} with the P_{O2}-dependent variable cooperativity hypothesis for O_2-Hb binding, and are shown in Fig. 4. The models of S_{HbO2} and S_{HbCO2} simulate the Bohr and Haldane effects, and the synergistic effects of 2,3-DPG and T on the HbO_2 and $HbCO_2$ dissociation curves. These simulations are consistent with the previous simulations by Dash and Bassingthwaighte (2010), except for their greater accuracy. The shifts in the HbO_2 dissociation curves seen in Figs. 4(E–H) are correlated with the variations in the P_{50} values plotted in Figs. 2(A–D) (solid lines), as defined by Eqs. 9(a–d) and validated by diverse experimental data in Figs. 3(A–D). Similarly, the shifts in the $HbCO_2$ dissociation curves seen in Figs. 4(I–L) are correlated with the extent of CO_2 binding to Hb under stipulated physiological conditions, as validated by diverse experimental data in Figs. 3(E–F). These simulations clearly show the different

effect of each variable on O_2 and CO_2 binding to Hb; pH is shown to significantly influence the O_2 and CO_2 binding, compared with the smaller effects of P_{CO2}, 2,3-DPG, and T.

The accurate and efficient numerical inversion of our refined S_{HbO2} model under standard physiological conditions is demonstrated in Fig. 5, based on the data of Severinghaus and colleagues (Roughton *et al.*, 1972; Roughton & Severinghaus, 1973; Severinghaus, 1979) and Winslow et al. (1977). The inset plots in Figs. 5A and 5B clearly show the improved agreement between the inverted P_{O2} values and the experimental P_{O2} values at lower S_{HbO2} levels (<40%) when the Hill coefficient nH is allowed to vary as a function P_{O2} according to Eq. 11, rather than being held constant. A similar conclusion may be drawn from Figs. 5C and 5D. The results for the inverse problem are consistent with the results for the forward problem shown in Fig. 1. The comprehensive simulations of the numerical inversions under varying physiological conditions are shown in Fig. 6. These include the simulations of P_{O2} as a function of S_{HbO2} and the simulations of P_{CO2} as a function of S_{HbCO2} over a wide range of values of the relevant physiological variables. In each scenario, three variables are fixed at their standard physiological levels, while the fourth one is allowed to increase by predetermined increments over a large range, as in the simulations for the forward problem in Fig. 4. It is apparent that our iterative numerical inversion schemes are able to effectively simulate P_{O2} and P_{CO2} levels from the S_{HbO2} and S_{HbCO2} levels over a wide range of physiological conditions.

Discussion

We have shown here how shifts in the HbO_2 dissociation curve due to variations in P_{CO2}, pH, 2,3-DPG, and T (where the variations occur in one variable at a time or several variables simultaneously) may be handled easily in the Hill equation by using an equation of state for P_{50} which incorporates the contribution from each of these four variables. While other equations exist for P_{50}, to the best of our knowledge, none incorporates contributions from all of the four variables under discussion or is as extensively validated using independent experimental data. Moreover, we believe that Eq. 10 is the most accurate equation of state for P_{50} currently available. Although standard versions of Hill's two-parameter equation for S_{HbO2} (using only P_{50} and nH) have been widely used in the past, it is recognized that when nH is set equal to 2.7, as is common practice, the equation is inaccurate for S_{HbO2} below 30 per cent and above 98 per cent (Dash & Bassingthwaighte, 2010), thus stimulating the development of improved descriptions by Adair (1925), Kelman (1966b), Severinghaus (1979), Siggaard-Andersen et al. (1984), Buerk and Bridges (1986), and others. In this paper, we have addressed this important deficiency in the standard Hill equation by expressing the Hill coefficient nH as a simple exponential function of P_{O2} (Eq. 11), with P_{50} given by Eq. 10. Figures 1, 3, and 5 show that this change improves the agreement between the model and available experimental data at both standard physiological conditions and at other values of pH, P_{CO2}, 2,3-DPG, and temperature that characterize pathophysiological states.

So the question that arises is this: Using these modifications, how does Hill's equation compare with other commonly used mathematical models of the HbO_2 dissociation curve? In Figs. 7A and 7C, we show the fit of our new refined Hill-based equation for S_{HbO2} to the

data of Severinghaus and colleagues (Roughton *et al.*, 1972; Roughton & Severinghaus, 1973; Severinghaus, 1979) under standard physiological conditions and compare that to the fit obtained using the S_{HbO2} models of Adair (1925), Kelman (1967), Buerk and Bridges (1986), Severinghaus (1979), and Siggaard-Andersen et al. (1984; 1990) for both the forward (computation of S_{HbO2} from P_{O2}) and inverse (computation of P_{O2} from S_{HbO2}) situations. The associated residual errors are shown in Figs. 7B and 7D. Although all the models shown in Fig. 7A seem to provide a good fit to the data (except for Kelman (1966b) for some P_{O2} values and Buerk and Bridges (1986) for high P_{O2}), the residual error shown in Fig. 7B is least for our present model and the models of Severinghaus (1979) and Siggaard-Andersen et al. (1984; 1990). Fig. 7C shows that all the models also produce a good fit to the data of Severinghaus and colleagues (Roughton *et al.*, 1972; Roughton & Severinghaus, 1973; Severinghaus, 1979) on inversion, but the error plotted in Fig. 7D indicates that our model is the most accurate for P_{O2} greater than $10^{0.5}$ (i.e. $P_{O2} > 3$) mmHg. Note that the distinction between the various models for the inverse problem is more apparent because of the use of a log-log scale. Apart from the two exceptions mentioned above, when compared with the data most of these models provide accuracy greater than 99.5% over the whole saturation range.

We also note here that the other S_{HbO2} models shown in Fig. 7 were parametrized based on the data of Severinghaus and colleagues (Roughton *et al.*, 1972; Roughton & Severinghaus, 1973; Severinghaus, 1979), and hence a comparison of the models with respect to the data of Winslow et al. (1977) cannot be made, unless they are re-parameterized. This is not the purpose of Fig. 7. Rather, the purpose of Fig. 7 is to illustrate how our new refined S_{HbO2} model is "at least" comparable in terms of accuracy to many other S_{HbO2} models used widely in the literature. Fig. 7 shows that this is indeed the case, yet our model is simpler than many others and efficiently invertible.

The recent model of Mateják et al. (2015), based on their version of the Adair equation (1925), is reported to fit well, the data of Severinghaus and colleagues (Roughton *et al.*, 1972; Roughton & Severinghaus, 1973; Severinghaus, 1979), and is also shown to fit the temperature and pH-dependent S_{HbO2} data of Reeves (1980) and Naeraa (1963), and carbaminohemoglobin data of Bauer and Schröder (1972) and Matthew (1977). Our present S_{HbO2} and S_{HbCO2} models fit these diverse data sets as accurately, and also fit the P_{CO2}, pH, and temperature-dependent data of Joels and Pugh (1958) and Hlastala et al. (1977), which were not used by Mateják et al. (18). Thus, the present S_{HbO2} and S_{HbCO2} models are well-validated based on a larger set of experimental data. More importantly, not only is our new refined S_{HbO2} model more accurate over the whole saturation range (important for the integrated computational modeling of alveolar-blood and blood-tissue O_2-CO_2 transport, exchange, and metabolism), it is also much simpler than our previous S_{HbO2} model, as there is no need to perform the complex computations to derive the indices n_1, n_2, n_3, and n_4.

The $HbCO_2$ dissociation curve is obtained in our treatment from Eq. 1b. The expression for K_{HbCO2} is derived from Eq. 3b and Eq. 4. When S_{HbO2} equals 1, K_{HbCO2} equals $K_3^{'}\Phi_2/\Phi_4$. Otherwise $K_4^{'}$ is required and is given by Eq. 7. Fortuitously, all the information regarding the variables P_{CO2}, pH, 2,3-DPG and T is contained in Eq. 10, the equation of state for P_{50}.

Thus, in our treatment, both S_{HbO2} and S_{HbCO2} rely on this equation for information about P_{CO2}, pH, 2,3-DPG and T. Other authors incorporate this information in different ways. For example, Severinghaus (1979) provides one equation for the temperature coefficient of P_{O2} and another for the change in $\ln P_{O2}$ per unit change in pH. If instead of equating Eq. 6 with Eq. 1a, we equate the Severinghaus equation for S_{HbO2} with Eq. 1a, we obtain the following expression for $K_4^{'}$:

$$K_4^{'}=\frac{\left(150+23400P_{O2}^2\right)\left(K_2^{'}\alpha_{CO2}P_{CO2}\Phi_1+\Phi_3\right)}{\alpha_{O2}\left(K_3^{'}\alpha_{CO2}P_{CO2}\Phi_2+\Phi_4\right)} \quad (12)$$

The value for P_{O2} used in Eq. 12 is that obtained after correction for temperature and pH. A similar approach may be adopted in the case of the Adair equation (Adair, 1925) to transfer information regarding pH, 2,3-DPG and T to the CO_2-Hb reaction system. Thus, Eq. 1b can be adapted for use with a variety of models of the HbO_2 dissociation curve.

Inversion of S_{HbO2} and S_{HbCO2} equations is an essential feature in modeling of alveolar-blood and blood-tissue O_2-CO_2 exchange at a sophisticated level. Algebraic inversion is possible with the Severinghaus S_{HbO2} equation (1979), but not in our models, once the Hill coefficient *nH* is allowed to vary. Iterative approaches are generally used for this. The Appendix provides fixed-point and quasi-Newton-Raphson iterative methods that would also be applicable to the models of Mateják et al. (2015) and others that are not analytically invertible.

Conclusions

We have simplified and extended our previously developed mathematical models of blood HbO_2 and $HbCO_2$ dissociation curves (Dash & Bassingthwaighte, 2010) to make them accurate over the whole saturation range for a wide range of values of P_{O2}, P_{CO2}, pH, 2,3-DPG, and temperature. The extended S_{HbO2} model features a P_{O2}-dependent variable Hill coefficient *nH* for the binding of O_2 to Hb, and incorporates a modified P_{50} model that provides accurate shifts in the HbO_2 dissociation curve over a wide range of physiological conditions, validated by diverse experimental data sets available in the literature. The information contained in this modified equation for P_{50} is transferred to the $HbCO_2$ dissociation curve via $K_4^{'}$, the apparent equilibrium constant in a single-step binding reaction of O_2 and Hb. The coupling of the Hb dissociation curves for O_2 and CO_2 may also be accomplished using models of S_{HbO2} other than the Hill equation. Finally, the extended S_{HbO2} and S_{HbCO2} models are conveniently invertible for efficient computation of P_{O2} from S_{HbO2} and P_{CO2} from S_{HbCO2}, using simple iterative numerical schemes with appropriate starting values that guarantee convergence. The calculations involved in our new S_{HbO2} and S_{HbCO2} models may be performed on handheld devices. More importantly, they can conveniently be used in the integrated computational modeling of alveolar-blood and blood-tissue O_2-CO_2 transport, exchange, and metabolism for analysis and mechanistic understanding of *in-vitro* and *in-vivo* blood gas data under physiological and non-

physiological conditions, such as ischemia and reperfusion, extremes in gas concentrations, high altitudes, and extreme temperatures.

Acknowledgments

We thank the reviewers for helpful and insightful comments that have enhanced the overall quality of the manuscript. This work was supported by the National Institute of Health Grants U01-HL122199, P50-GM094503, and P01-GM066730. The extension of P_{50} model to extreme/wider physiological conditions (e.g. pH > 8.5) was motivated by RKD's email correspondence with Stefan Kleiser (University Hospital Zurich), a user of the 2010 Dash and Bassingthwaighte S_{HbO2} and S_{HbCO2} models.

Frequently Used Abbreviations

α_{O2}	Solubility of oxygen
α_{CO2}	Solubility of carbon dioxide
$[O_2]$	Concentration of free oxygen
$[CO_2]$	Concentration of free carbon dioxide
$[H^+]$	Concentration of hydrogen ions (protons)
[DPG]	Concentration of 2,3-diphosphoglycerate (2,3-DPG)
T	Temperature
pH	$-\log_{10}([H^+])$
P_{O2}	Partial pressure of oxygen
P_{CO2}	Partial pressure of carbon dioxide
P_{50}	Partial pressure of oxygen for 50% HbO_2 saturation
Hb	Hemoglobin
HbO_2	Oxyhemoglobin
$HbCO_2$	Carbaminohemoglobin
K_{HbO2}	Apparent equilibrium constant of hemoglobin and oxygen binding
K_{HbCO2}	Apparent equilibrium constant of hemoglobin and carbon dioxide binding
S_{HbO2}	Saturation of hemoglobin with oxygen
S_{HbCO2}	Saturation of hemoglobin with carbon dioxide

References

Adair GS. The hemoglobin system VI. The oxygen dissociation curve of hemoglobin. J Biol Chem. 1925; 63:529–545.

Austin WH, Lacombe E, Rand PW, Chatterjee M. Solubility of carbon dioxide in serum from 15 to 38 C. Journal of Applied Physiology. 1963; 18:301–304. [PubMed: 13965591]

Bassingthwaighte JB, Beard DA, Carlson BE, Dash RK, Vinnakota K. Modeling to link regional myocardial work, metabolism and blood flows. Annals of biomedical engineering. 2012; 40:2379–2398. [PubMed: 22915334]

Bauer C, Schroder E. Carbamino compounds of haemoglobin in human adult and foetal blood. The Journal of Physiology. 1972; 227:457–471. [PubMed: 4647257]

Buerk DG, Bridges EW. A simplified algorithm for computing the variation in oxyhemoglobin saturation with pH, PCO_2, T and DPG. Chemical Engineering Communication. 1986; 47:113–124.

Dash RK, Bassingthwaighte JB. Blood HbO_2 and $HbCO_2$ dissociation curves at varied O_2, CO_2, pH, 2,3-DPG and temperature levels. Annals of Biomedical Engineering. 2004; 32:1676–1693. [PubMed: 15682524]

Dash RK, Bassingthwaighte JB. Simultaneous blood-tissue exchange of oxygen, carbon dioxide, bicarbonate, and hydrogen ion. Annals of Biomedical Engineering. 2006; 34:1129–1148. [PubMed: 16775761]

Dash RK, Bassingthwaighte JB. Erratum to: Blood HbO_2 and $HbCO_2$ dissociation curves at varied O_2, CO_2, pH, 2,3-DPG and temperature levels. Annals of Biomedical Engineering. 2010; 38:1683–1701. [PubMed: 20162361]

Forster RE, Constantine HP, Craw MR, Rotman HH, Klocke RA. Reaction of CO2 with human hemoglobin solution. The Journal of biological chemistry. 1968; 243:3317–3326. [PubMed: 5656372]

Geers C, Gros G. Carbon dioxide transport and carbonic anhydrase in blood and muscle. Physiol Rev. 2000; 80:681–715. [PubMed: 10747205]

Heath, MT. Scientific Computing: An Introductory Survey. The McGraw-Hill Companies, Inc; Boston: 2002.

Hedley-Whyte J, Laver MB. O_2 Solubility in Blood and Temperature Correction Factors for PO_2. Journal of Applied Physiology. 1964; 19:901–906. [PubMed: 14207742]

Hlastala MP, Woodson RD, Wranne B. Influence of temperature on hemoglobin-ligand interaction in whole blood. J Appl Physiol Respir Environ Exerc Physiol. 1977; 43:545–550. [PubMed: 21154]

Joels N, Pugh LG. The carbon monoxide dissociation curve of human blood. The Journal of Physiology. 1958; 142:63–77. [PubMed: 13564419]

Kelman GR. Calculation of certain indices of cardio-pulmonary function, using a digital computer. Respir Physiol. 1966a; 1:335–343. [PubMed: 5968348]

Kelman GR. Digital computer subroutine for the conversion of oxygen tension into saturation. Journal of Applied Physiology. 1966b; 21:1375–1376. [PubMed: 5916678]

Kelman GR. Digital computer procedure for the conversion of PCO_2 into blood CO_2 content. Respir Physiol. 1967; 3:111–115. [PubMed: 6059098]

Matejak M, Kulhanek T, Matousek S. Adair-based hemoglobin equilibrium with oxygen, carbon dioxide and hydrogen ion activity. Scand J Clin Lab Invest. 2015; 75:113–120. [PubMed: 25594800]

Matthew JB, Morrow JS, Wittebort RJ, Gurd FR. Quantitative determination of carbamino adducts of alpha and beta chains in human adult hemoglobin in presence and absence of carbon monoxide and 2,3-diphosphoglycerate. The Journal of biological chemistry. 1977; 252:2234–2244. [PubMed: 14958]

Naeraa N, Petersen ES, Boye E. The influence of simultaneous, independent changes in pH and carbon dioxide tension on the in vitro oxygen tension-saturation relationship of human blood. Scand J Clin Lab Invest. 1963; 15:141–151. [PubMed: 13937062]

Pozrikidis, C. Numerical Computations in Science and Engineering. Oxford University Press; New York: 2008.

Rees SE, Andreassen S. Mathematical models of oxygen and carbon dioxide storage and transport: the acid-base chemistry of blood. Crit Rev Biomed Eng. 2005; 33:209–264. [PubMed: 15833078]

Reeves RB. The effect of temperature on the oxygen equilibrium curve of human blood. Respir Physiol. 1980; 42:317–328. [PubMed: 6784210]

Rossi-Bernardi L, Roughton FJ. The specific influence of carbon dioxide and carbamate compounds on the buffer power and Bohr effects in human haemoglobin solutions. The Journal of Physiology. 1967; 189:1–29. [PubMed: 16992238]

Roughton FJ, Severinghaus JW. Accurate determination of O_2 dissociation curve of human blood above 98.7 percent saturation with data on O_2 solubility in unmodified human blood from 0 degrees to 37 degrees C. Journal of Applied Physiology. 1973; 35:861–869. [PubMed: 4765824]

Roughton, FJW.; Deland, EC.; Kernohan, JC.; Severinghaus, JW. Some recent studies of the oxyhemoglobin dissociation curve of human blood under physiological conditions and the fitting

of the Adair equation to the standard curve. In: Rørth, M.; Astrup, P., editors. Proceedings of the Oxygen Affinity of Hemoglobin and Red Cell Acid Base Status; Proceedings of the Alfred Benzon Symposium IV Held at the Premises of the Royal Danish Academy of Sciences and Letters; City. p. 73-81.(Year)

Severinghaus JW. Simple, accurate equations for human blood O_2 dissociation computations. J Appl Physiol Respir Environ Exerc Physiol. 1979; 46:599–602. [PubMed: 35496]

Siggaard-Andersen O. Oxygen-linked hydrogen ion binding of human hemoglobin. Effects of carbon dioxide and 2,3-diphosphoglycerate. I. Studies on erythrolysate. Scand J Clin Lab Invest. 1971; 27:351–360. [PubMed: 5556604]

Siggaard-Andersen O, Garby L. The Bohr effect and the Haldane effect. Scand J Clin Lab Invest. 1973; 31:1–8. [PubMed: 4687773]

Siggaard-Andersen O, Rorth M, Norgaard-Pedersen B, Andersen OS, Johansen E. Oxygen-linked hydrogen ion binding of human hemoglobin. Effects of carbon dioxide and 2,3-diphosphoglycerate. IV. Thermodynamical relationship between the variables. Scand J Clin Lab Invest. 1972a; 29:303–320. [PubMed: 5037628]

Siggaard-Andersen O, Salling N. Oxygen-linked hydrogen ion binding of human hemoglobin. Effects of carbon dioxide and 2,3-diphosphoglycerate. II. Studies on whole blood. Scand J Clin Lab Invest. 1971; 27:361–366. [PubMed: 5556605]

Siggaard-Andersen O, Salling N, Norgaard-Pedersen B, Rorth M. Oxygen-linked hydrogen ion binding of human hemoglobin. Effects of carbon dioxide and 2,3-diphosphoglycerate. Scand J Clin Lab Invest. 1972b; 29:185–193. [PubMed: 5029322]

Siggaard-Andersen O, Siggaard-Andersen M. The oxygen status algorithm: a computer program for calculating and displaying pH and blood gas data. Scand J Clin Lab Invest Suppl. 1990; 203:29–45. [PubMed: 2128561]

Siggaard-Andersen O, Wimberley PD, Gothgen I, Siggaard-Andersen M. A mathematical model of the hemoglobin-oxygen dissociation curve of human blood and of the oxygen partial pressure as a function of temperature. Clin Chem. 1984; 30:1646–1651. [PubMed: 6478594]

Tyuma I. The Bohr effect and the Haldane effect in human hemoglobin. The Japanese journal of physiology. 1984; 34:205–216. [PubMed: 6433091]

von Restorff W, Holtz J, Bassenge E. Exercise induced augmentation of myocardial oxygen extraction in spite of normal coronary dilatory capacity in dogs. Pflugers Archiv : European journal of physiology. 1977; 372:181–185. [PubMed: 564040]

Winslow RM, Samaja M, Winslow NJ, Rossi-Bernardi L, Shrager RI. Simulation of continuous blood O_2 equilibrium curve over physiological pH, DPG, and PCO_2 range. J Appl Physiol Respir Environ Exerc Physiol. 1983; 54:524–529. [PubMed: 6403493]

Winslow RM, Swenberg ML, Berger RL, Shrager RI, Luzzana M, Samaja M, Rossi-Bernardi L. Oxygen equilibrium curve of normal human blood and its evaluation by Adair's equation. The Journal of biological chemistry. 1977; 252:2331–2337. [PubMed: 849931]

Wolf MB. Whole body acid-base and fluid-electrolyte balance: a mathematical model. American journal of physiology. Renal physiology. 2013; 305:F1118–1131. [PubMed: 23884137]

Appendix: Efficient Iterative Schemes for Numerical Computations of PO2 from SHbO2 and PCO2 from SHbCO2

Two efficient numerical methods are presented below for the inversion of P_{O2} from S_{HbO2} and P_{CO2} from S_{HbCO2}, based on fixed-point and quasi-Newton-Raphson iteration methods (Scheme-1 and Scheme-2, respectively) (Heath, 2002; Pozrikidis, 2008).

The iterative schemes for the computation of P_{O2} from S_{HbO2} are given by:

$$\text{Scheme}-1: P_{O2}^{New} = P_{50}\left(\frac{S_{HbO2}^{Input}}{1-S_{HbO2}^{Input}}\right)^{\frac{1}{nH(P_{O2}^{Old})}} \quad \text{(A-1a)}$$

$$\text{Scheme}-2: P_{O2}^{New} = P_{O2}^{Old} - \left(\frac{S_{HbO2}(P_{O2}^{Old}) - S_{HbO2}^{Input}}{S'_{HbO2}(P_{O2}^{Old})}\right) = P_{O2}^{Old} - \left(\frac{0.02P_{O2}^{Old}\left(S_{HbO2}(P_{O2}^{Old}) - S_{HbO2}^{Input}\right)}{S_{HbO2}(P_{O2}^{Old}+0.01P_{O2}^{Old}) - S_{HbO2}(P_{O2}^{Old}-0.01P_{O2}^{Old})}\right) \quad \text{(A-1b)}$$

where S_{HbO2}^{Input} is the input S_{HbO2} (given), $S_{HbO2}(P_{O2}^{Old})$ is the value of S_{HbO2} evaluated at P_{O2}^{Old}, and $S'_{HbO2}(P_{O2}^{Old})$ is the derivative of S_{HbO2} w.r.t. P_{O2} evaluated at P_{O2}^{Old}. Either Eq. 1a or Eq. 6 can be used as the expression for S_{HbO2}. In the second version of Eq. A-1b, it is only necessary to perform function evaluation, because $S'_{HbO2}(P_{O2}^{Old})$ has been estimated using a central-difference formula for first-order derivatives (Pozrikidis, 2008), which eliminates the need to differentiate the expression for S_{HbO2}, which may be complicated. If the Hill coefficient *nH* is held constant, Eq. A-1a itself provides the analytical inversion for the computation of P_{O2} from S_{HbO2}. For P_{O2}-dependent *nH* (Eq. 11), the iteration scheme of Eq. A-1a converges within 3 to 5 iterations with 10^{-3} accuracy, using any starting value for P_{O2}. For the same accuracy, the iteration scheme of Eq. A-1b converges within 5 to 8 iterations using P_{50} from Eq. 10 as the starting value for P_{O2}.

The analogous iterative schemes for the computation of P_{CO2} from S_{HbCO2} are given by:

$$\text{Scheme}-1: P_{CO2}^{New} = \left(\frac{S_{HbCO2}^{Input}}{1-S_{HbCO2}^{Input}}\right)\left(\frac{1}{\alpha_{CO2}K_{HbCO2}(P_{CO2}^{Old})}\right) \quad \text{(A-2a)}$$

$$\text{Scheme}-2: P_{CO2}^{New} = P_{CO2}^{Old} - \left(\frac{S_{HbCO2}(P_{CO2}^{Old}) - S_{HbCO2}^{Input}}{S'_{HbCO2}(P_{CO2}^{Old})}\right) = P_{CO2}^{Old} - \left(\frac{0.02P_{CO2}^{Old}\left(S_{HbCO2}(P_{CO2}^{Old}) - S_{HbCO2}^{Input}\right)}{S_{HbCO2}(P_{CO2}^{Old}+0.01P_{CO2}^{Old}) - S_{HbCO2}(P_{CO2}^{Old}-0.01P_{CO2}^{Old})}\right) \quad \text{(A-2b)}$$

Similar iterative methods can be used to compute P_{O2} from total $[O_2]$ and P_{CO2} from total $[CO_2]$. Note that the total $[O_2]$ and the total $[CO_2]$ are defined in Table 1.

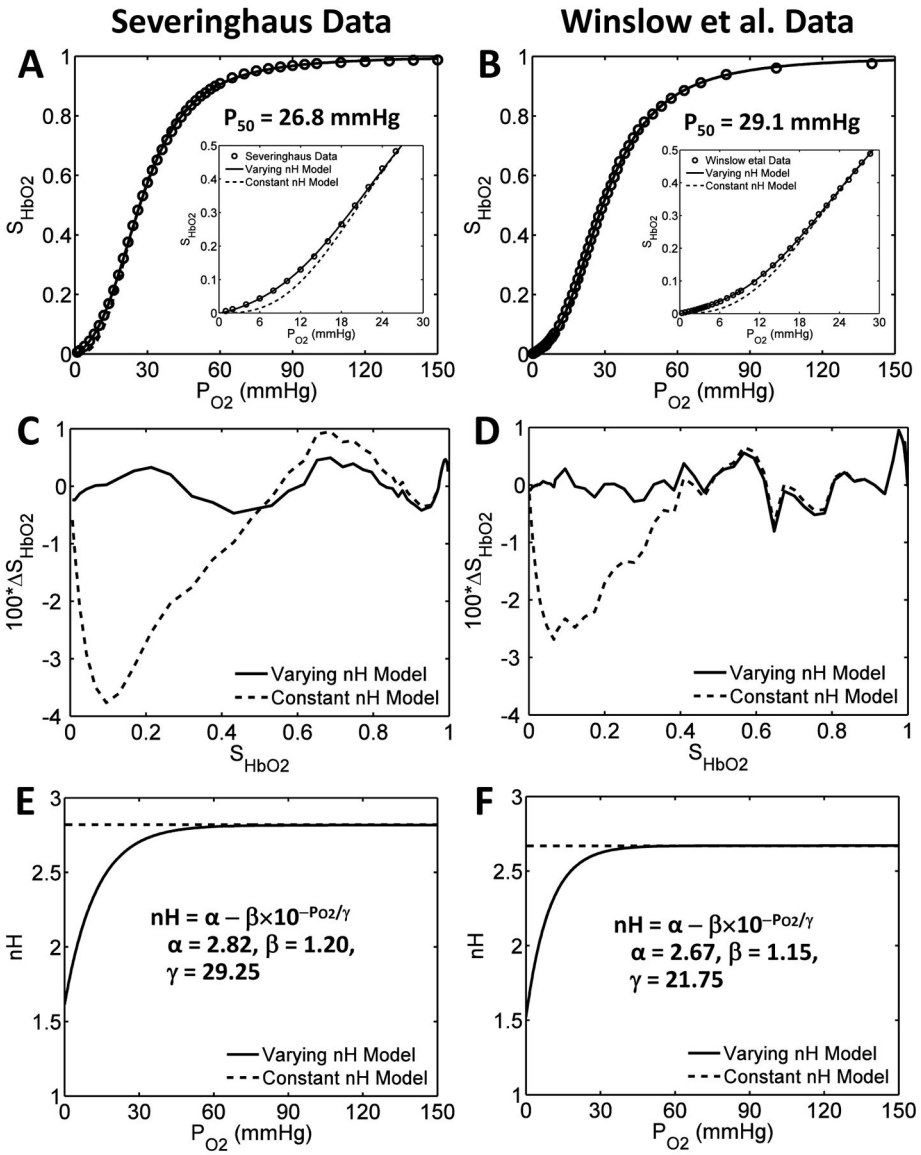

Figure 1. Illustration of the accuracy of the modified S_{HbO2} model under standard physiological conditions with P_{O2}-dependent variable cooperativity hypothesis for O_2-Hb binding

(A,B) Comparison of the model-simulated HbO_2 dissociation curves with constant and variable cooperativity hypotheses for O_2-Hb binding (constant and variable Hill coefficient *nH*) to available experimental data in the literature, on normal human blood at standard physiological conditions. The simulations in panel A are compared to the data of Severinghaus and colleagues (Roughton *et al.*, 1972; Roughton & Severinghaus, 1973; Severinghaus, 1979), and those in panel B are compared to the data of Winslow et al. (1977). The simulations in the main plots are compared to the data over the whole S_{HbO2} range, while those in the inset plots are compared to the data for $S_{HbO2} \leq 0.5$, effectively demonstrating the improved accuracy of the modified S_{HbO2} model with variable *nH* in simulating the data in the lower S_{HbO2} range. (**C,D**) The percentage deviations ($100 \times \Delta S_{HbO2}$) of the model-simulated S_{HbO2} values from the experimental S_{HbO2} values for the

constant and variable *nH* models plotted as functions of S_{HbO2} for the data of Severinghaus and colleagues (Roughton *et al.*, 1972; Roughton & Severinghaus, 1973; Severinghaus, 1979) and Winslow et al. (1977). The incorporation of the variable cooperativity hypothesis for O_2-Hb binding (variable *nH*) has improved the accuracy of the S_{HbO2} model. (**E,F**) The P_{O2}-dependent variation of *nH* corresponding to the constant and variable cooperativity hypotheses for O_2-Hb binding that are obtained based on fittings of the modified S_{HbO2} model to the data of Severinghaus and colleagues (Roughton *et al.*, 1972; Roughton & Severinghaus, 1973; Severinghaus, 1979) and Winslow et al. (1977). The insets in plots (E,F) show the expressions for the variable *nH* and the governing parameter values for the two data sets.

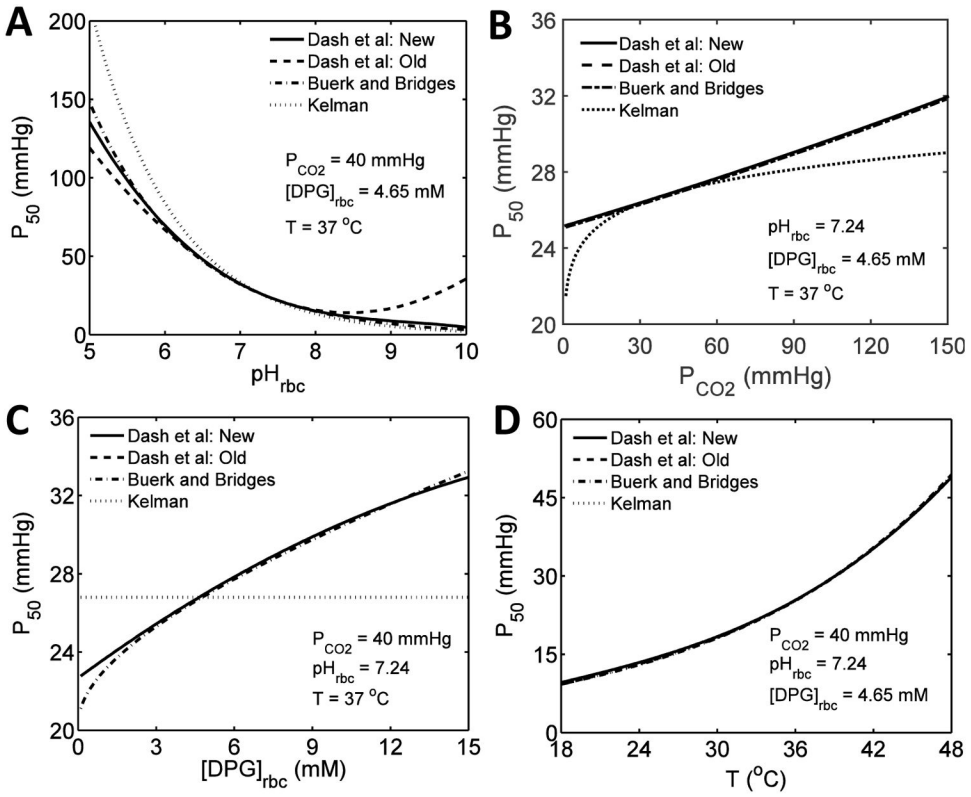

Figure 2. Comparison of P_{50} values under various physiological conditions based on simulations of different P_{50} models

(A–D) Comparison of the modified P_{50} model (Eqs. 9 and 10) with the previous P_{50} models from the literature (Kelman, 1966b; Buerk & Bridges, 1986; Dash & Bassingthwaighte, 2010), in which the model-simulated P_{50} values are plotted as functions of one variable with the other variables fixed at their standard physiological values; i.e. P_{50} as a function of pH_{rbc} (A), P_{CO2} (B), $[DPG]_{rbc}$ (C), and T (D). The P_{50} values have been computed from Eqs. 9 and 10 under varying physiological conditions with appropriate multiplicative factors (0.833, 0.588 and 1.02 for $P_{50,\Delta pH}$, $P_{50,\Delta CO2}$ and $P_{50,\Delta T}$, respectively) to allow a comparison with the previous models, which have not been adjusted to account for the data of Joels and Pugh (1958), Naeraa et al. (1963), Hlastala et al. (1977) and Reeves (1980).

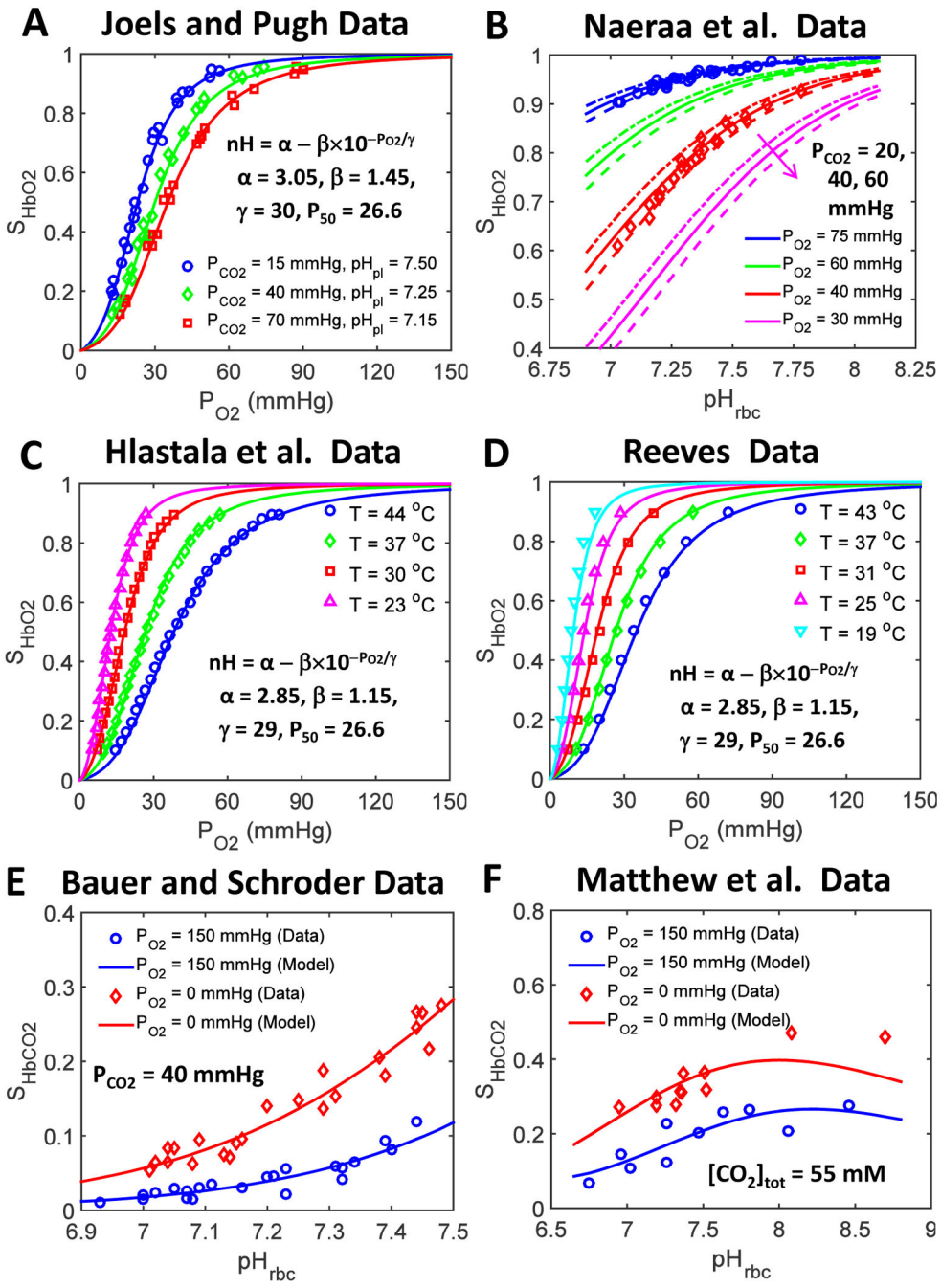

Figure 3. Comparison of our improved S_{HbO2} and S_{HbCO2} model simulations to the diverse experimental data available in the literature under non-standard physiological conditions

(A) HbO_2 dissociation curves obtained from our improved S_{HbO2} model (i.e. modified S_{HbO2} model with variable cooperativity hypothesis for O_2-Hb binding (variable *nH*)) compared with the data of Joels and Pugh (1958) obtained at various pH_{pl} and P_{CO2} levels with T = 37 °C. The inset shows the expression for the variable *nH* and the governing parameter values that produce the best fit of the model to these data sets. In addition, these model fittings characterize the pH and P_{CO2} dependencies of P_{50} in Eqs. 9a and 9b. (**B**)

S_{HbO2} levels obtained from our improved S_{HbO2} model compared to the data of Naeraa et al. (1963) obtained as a function of pH_{rbc} for different P_{O2} and P_{CO2} levels at 37 °C. Other details are as for panel A. (**C,D**) HbO_2 dissociation curves obtained from our improved S_{HbO2} model compared with the data of Hlastala et al. (1977) and Reeves (1980) obtained for various values of T with pH_{pl} and P_{CO2} fixed at 7.4 and 40 mmHg, respectively. The insets show the expression for the variable nH and the governing parameter values that enable best fits of the model to these data sets. In addition, these model fittings characterize the temperature dependency of P_{50} in Eq. 9d. (**E,F**) S_{HbCO2} levels obtained from our improved S_{HbCO2} model compared with the data of Bauer and Schröder (1972) and Matthew et al. (1977) obtained as a function of pH_{rbc} in the oxygenated (high P_{O2}) and deoxygenated (zero P_{O2}) blood with P_{CO2} fixed at 40 mmHg (T = 37 °C) in the former experiments and total $[CO_2]$ fixed at 55 mM (T = 30 °C) in the latter experiments. These model fittings provide the estimates of the equilibrium constants associated with the binding of CO_2 to oxygenated and deoxygenated Hb as well as the ionization constants of oxygenated and deoxygenated Hb.

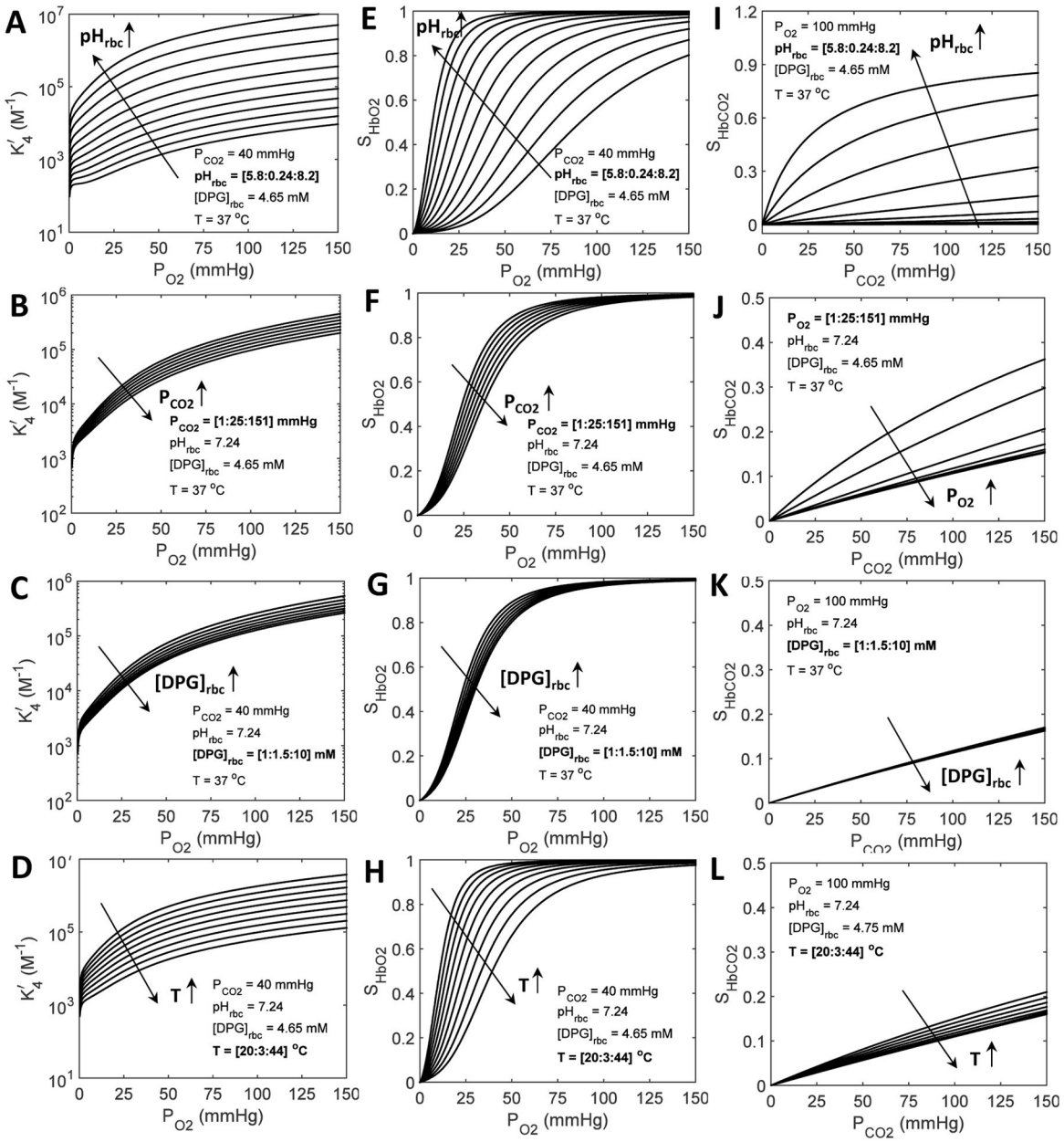

Figure 4. Simulations of the apparent HbO_2 binding constant K_4' (A–D), HbO_2 dissociation curves (E–H), and $HbCO_2$ dissociation curves (I–L) under varying physiological conditions based on our modified models of K_4', S_{HbO2} and S_{HbCO2} with the P_{O2}-dependent variable cooperativity hypothesis for O_2-Hb binding

In plots (A–D) and (E–H), the simulations of K_4' and S_{HbO2} are shown as functions of P_{O2}, respectively, while in plots (I–L), the simulations of S_{HbCO2} are shown as a function of P_{CO2}. The values of the variables used in each simulation are shown as insets in each panel. Three of the variables are fixed at their standard physiological values, while the fourth one is allowed to increase from a low value to a high value by predetermined increments, shown by the sequence [low: increment: high]. Specifically, in plots (A,E,I), pH_{rbc} varies, while either P_{CO2} or P_{O2}, $[DPG]_{rbc}$ and T are fixed; in plots (B,F,J), either P_{CO2} or P_{O2} varies,

while pH_{rbc}, $[DPG]_{rbc}$ and T are fixed; in plots (C,G,K), $[DPG]_{rbc}$ varies, while pH_{rbc}, either P_{CO2} or P_{O2}, and T are fixed; in plots (D,H,L), T varies, while pH_{rbc}, either P_{O2} or P_{CO2}, and $[DPG]_{rbc}$ are fixed. In each plot, the long arrow shows the direction of the shift produced by increasing the value of the fourth variable. The shifts in the HbO_2 dissociation curves seen in plots (E–H) are correlated with the variations in the P_{50} values plotted in Figs. 2(A–D) (solid lines), as defined by Eqs. 9(a–d) and validated by diverse experimental data in Figs. 3(A–D). Similarly, the shifts in the $HbCO_2$ dissociation curves seen in plots (I–L) are correlated with the extent of CO_2 binding with Hb under stipulated physiological conditions, as validated by diverse experimental data in Figs. 3(E–F).

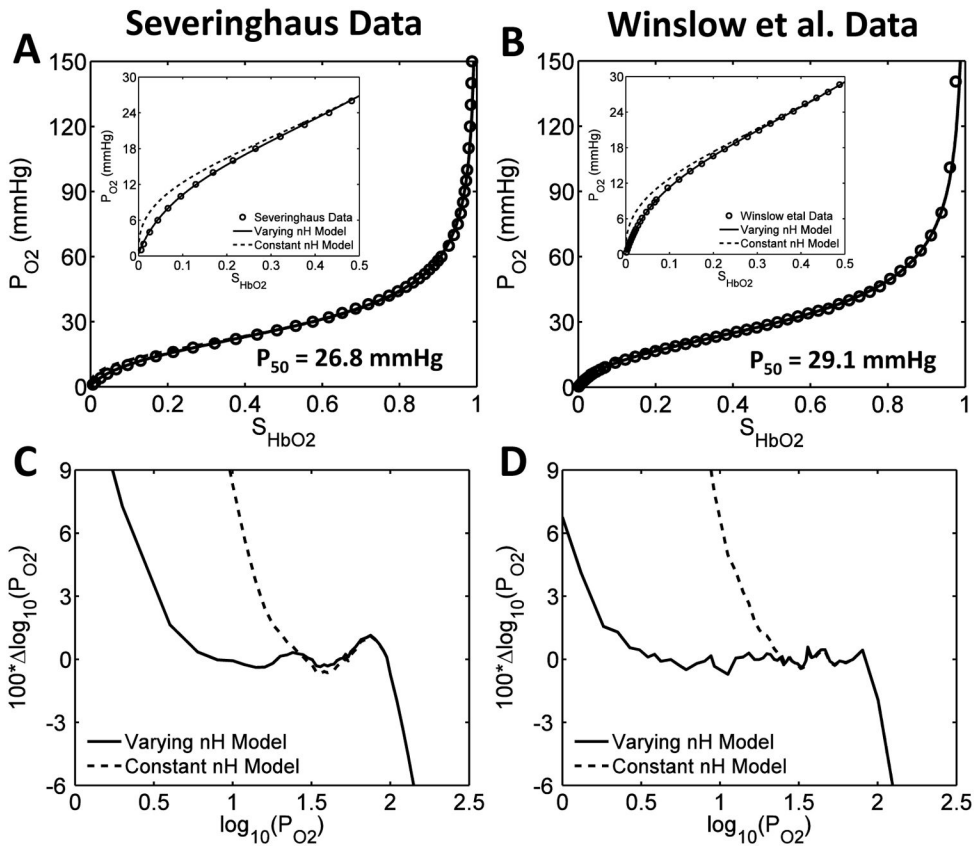

Figure 5. Illustration of the accurate numerical inversion of the modified S_{HbO2} model under standard physiological conditions with the P_{O2}-dependent variable cooperativity hypothesis for O_2-Hb binding

(A,B) Comparison of the numerically-inverted P_{O2} values from the S_{HbO2} values with constant and variable cooperativity hypotheses for O_2-Hb binding (constant and variable Hill coefficient *nH*) to available experimental data in the literature on normal human blood at standard physiological conditions. The numerical inversions in panel A are compared to the data of Severinghaus and colleagues (Roughton *et al.*, 1972; Roughton & Severinghaus, 1973; Severinghaus, 1979), and those in panel B are compared to the data of Winslow et al. (1977). The numerical inversions in the main plots are compared to the data over the whole S_{HbO2} range, while those in the inset plots are compared to the data for $S_{HbO2} \leq 0.5$, effectively demonstrating the accurate numerical inversion of the modified S_{HbO2} model with variable *nH* in simulating the data in the lower S_{HbO2} range. (**C,D**) The percentage deviations ($100 \times \Delta\log_{10}(P_{O2})$) of the numerically-inverted $\log_{10}(P_{O2})$ values from the experimental $\log_{10}(P_{O2})$ values for the constant and variable *nH* models plotted as functions of $\log_{10}(P_{O2})$ for the data of Severinghaus and colleagues (Roughton *et al.*, 1972; Roughton & Severinghaus, 1973; Severinghaus, 1979) and Winslow et al. (1977). The P_{O2} dependencies of *nH* for these two data sets are as shown in Figs. 1(E,F). The incorporation of the variable cooperativity hypothesis for O_2-Hb binding (variable *nH*) has improved the accuracy of the numerically-inverted P_{O2} values from the S_{HbO2} values.

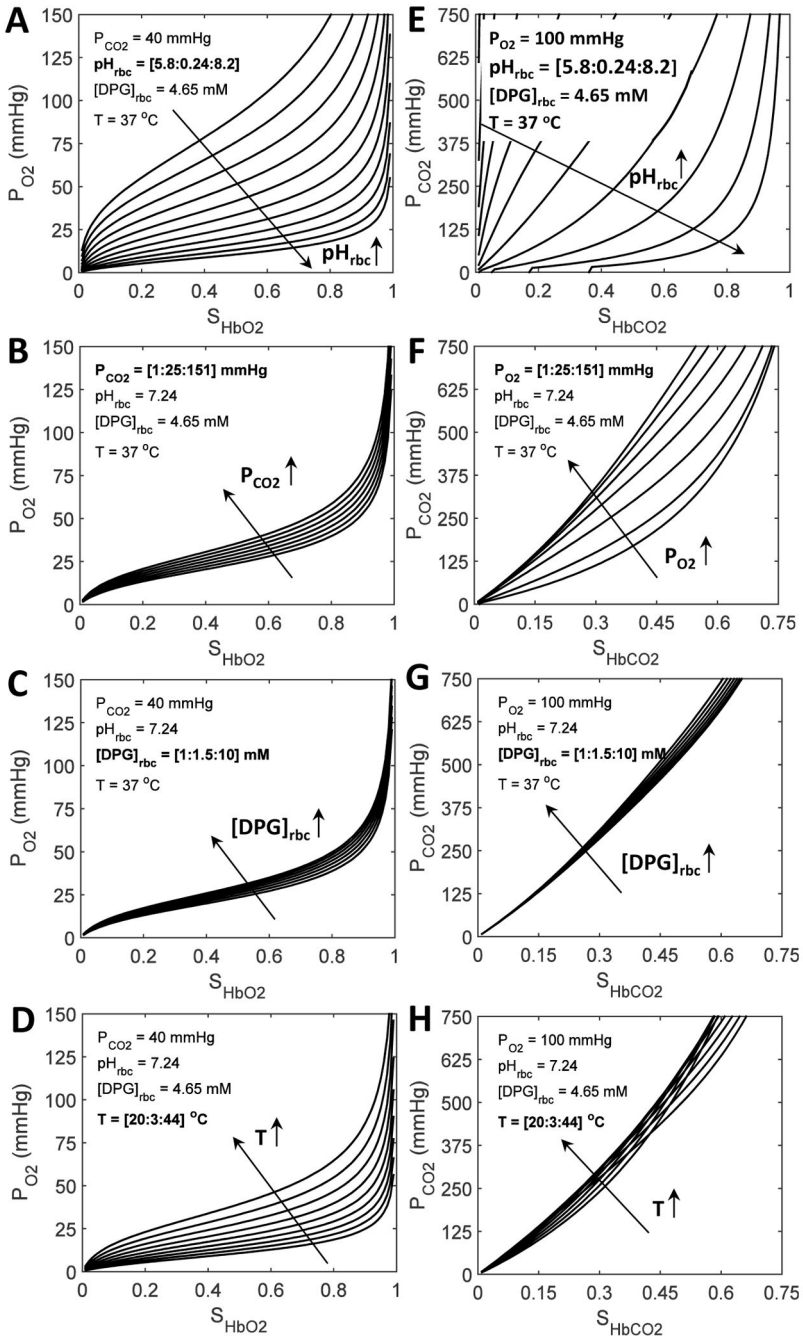

Figure 6. Illustration of the effective numerical inversion of our improved S_{HbO2} and S_{HbCO2} equations under varying physiological conditions

In plots (A–D), the simulations of P_{O2} as a function of S_{HbO2} are shown, while in plots (E–H), the simulations of P_{CO2} as a function of S_{HbCO2} are shown. In each scenario, three variables are fixed at their standard physiological levels, while the fourth one is allowed to increase by predetermined increments over a large range, as described in detail in the legend to Fig. 4. The inversion computations were carried out using a variant of the Newton-Raphson method (i.e. quasi-Newton-Raphson method) with appropriate initial guesses that guaranteed convergence. These plots are the mirror-images of the corresponding plots in

Fig. 4 (but with different scales), illustrating the accuracy of the numerical inversion schemes.

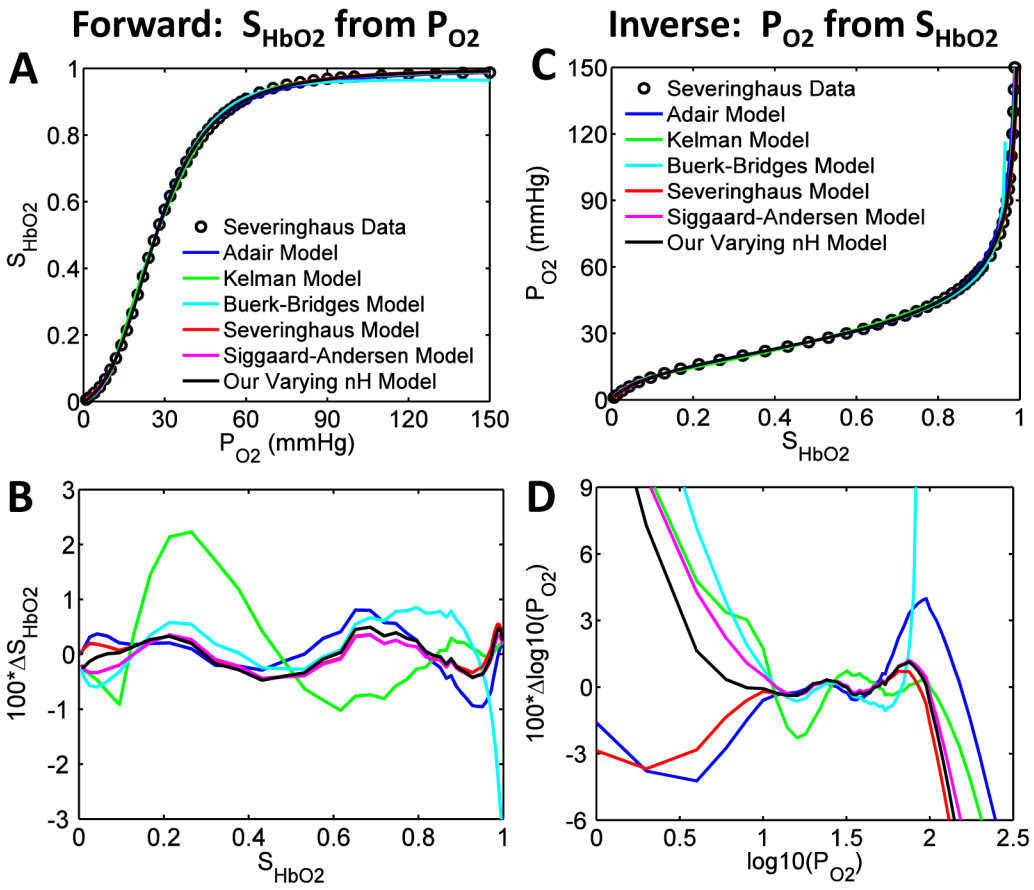

Figure 7. Comparison of our improved S_{HbO2} model with alternative S_{HbO2} models from the literature in simulating available experimental data at standard physiological conditions (both forward and inverse problems)

In each case, the model for comparison has first been parametrized to produce a "best fit" based on the experimental data. **(A)** HbO_2 dissociation curves obtained from our improved S_{HbO2} model compared with those obtained from other commonly used S_{HbO2} models (Adair, 1925; Kelman, 1966b; Severinghaus, 1979; Siggaard-Andersen *et al.*, 1984; Buerk & Bridges, 1986), in simulating the data of Severinghaus and colleagues (Roughton *et al.*, 1972; Roughton & Severinghaus, 1973; Severinghaus, 1979) on normal human blood at standard physiological conditions. (**B**) The percentage deviations ($100 \times \Delta S_{HbO2}$) of the model-simulated S_{HbO2} values from the experimental S_{HbO2} values based on our improved S_{HbO2} model and the alternative models, plotted as functions of S_{HbO2} for the data of Severinghaus and colleagues (Roughton *et al.*, 1972; Roughton & Severinghaus, 1973; Severinghaus, 1979). (**C**) Comparisons of the numerically-inverted P_{O2} values from the S_{HbO2} values obtained from our improved S_{HbO2} model and the alternative models, in simulating the data of Severinghaus and colleagues (Roughton *et al.*, 1972; Roughton & Severinghaus, 1973; Severinghaus, 1979) on normal human blood at standard physiological conditions. (**D**) The percentage deviations ($100 \times \Delta \log_{10}(P_{O2})$) of the numerically-inverted $\log_{10}(P_{O2})$ values from the experimental $\log_{10}(P_{O2})$ values based on our improved S_{HbO2} model and the alternative S_{HbO2} models, plotted as functions of $\log_{10}(P_{O2})$ for the data of Severinghaus and colleagues (Roughton *et al.*, 1972; Roughton & Severinghaus, 1973;

Severinghaus, 1979). The comparison may be repeated using the data of Winslow et al. (1977). This involves the re-parametrization of each model to obtain the best fit to the data. The result has not been shown here as it does not contribute anything further to the conclusions already drawn.

Table 1

Model parameter values used in the simulations, most of which are as presented in the Dash and Bassingthwaighte (2010) paper; model parameters that are re-estimated based on fittings of the model to the experimental data in Figs. 1 and 3 are shown with footnotes. Unless otherwise noted, the kinetic parameter values are at T = 37 °C.

Parameter	Definition	Value	Unit
K_1''	Ionization constant of H_2CO_3	5.5×10^{-4}	M
K_1'	Equilibrium constant for the CO_2 hydration reaction: $CO_2+H_2O \leftrightarrow H_2CO_3\ (K_1'=K_1/K_1'')$	1.4×10^{-3}	Unitless
K_1	Equilibrium constant for the overall CO_2 hydration reaction: $CO_2+H_2O \leftrightarrow HCO_3^-+H^+\ (K_1=K_1'\cdot K_1'')$; $pK_1 = -\log_{10}(K_1) = 6.1 - 0.0434(pH_{pl}-7.4) + 0.0014(T-37)(pH_{pl}-7.4)$	7.94×10^{-7} (pH_{pl} = 7.4; T = 37°C)	M
K_2''	Ionization constant of HbNHCOOH	1×10^{-6}	M
K_2'	Equilibrium constant for the CO_2-Hb binding reaction: $CO_2+HbNH_2 \leftrightarrow HbNHCOOH\ (K_2'=K_2/K_2'')$	21.5[#] 23.65[*]	M^{-1}
K_2	Equilibrium constant for the overall CO_2-Hb binding reaction: $CO_2+HbNH_2 \leftrightarrow HbNHCOO^-+H^+\ (K_2=K_2'\cdot K_2'')$	21.5×10^{-6}[#] 23.65×10^{-6}[*]	Unitless
K_3''	Ionization constant of $HbO_2NHCOOH$	1×10^{-6}	M
K_3'	Equilibrium constant for the CO_2-HbO_2 binding reaction: $CO_2+HbO_2NH_2 \leftrightarrow HbO_2NHCOOH\ (K_3'=K_3/K_3'')$	11.3[#] 14.7[*]	M^{-1}
K_3	Equilibrium constant for the overall CO_2-HbO_2 binding reaction: $CO_2+HbO_2NH_2 \leftrightarrow HbO_2NHCOO^-+H^+\ (K_3=K_3'\cdot K_3'')$	11.3×10^{-6}[#] 14.7×10^{-6}[*]	Unitless
$K_{4,S}'$	Equilibrium constant for the overall O_2-Hb binding reaction: $O_2 + HbNH_2 \leftrightarrow HbO_2NH_2$ at standard physiological conditions (otherwise it is a function of P_{O2}, P_{CO2}, pH_{rbc}, $[DPG]_{rbc}$ and T)	2.03×10^5	M^{-1}
K_5''	Ionization constant of $HbNH_3^+$	2.4×10^{-8}[#] 2.64×10^{-8}[*]	M
K_6''	Ionization constant of $HbO_2NH_3^+$	1.2×10^{-8}[#] 1.56×10^{-8}[*]	M
nH	Hill coefficient with variable cooperativity hypothesis for O_2 binding to Hb: $nH = \alpha - \beta\times10^{-P_{O2}/\gamma}$ (Eq. 11)	Variable	Unitless
α	Parameter governing P_{O2}-dependent variable Hill coefficient nH with variable cooperativity hypothesis for O_2 binding to Hb	2.82[$]	Unitless
β	Parameter governing P_{O2}-dependent variable Hill coefficient nH with variable cooperativity hypothesis for O_2 binding to Hb	1.20[$]	Unitless
γ	Parameter governing P_{O2}-dependent variable Hill coefficient nH with variable cooperativity hypothesis for O_2 binding to Hb	29.25[$]	mmHg

Parameter	Definition	Value	Unit
$P_{50,S}$	Level of P_{O2} at which Hb is 50% saturated by O_2 at standard physiological levels of P_{CO2}, pH_{rbc}, $[DPG]_{rbc}$ and T	26.8[$]	mmHg
$P_{O2,S}$	Standard partial pressure of O_2 in blood	100	mmHg
$P_{CO2,S}$	Standard partial pressure of CO_2 in blood	40	mmHg
$pH_{pl,S}$	Standard pH in plasma	7.4	Unitless
$pH_{rbc,S}$	Standard pH in RBCs, related to the standard plasma pH by: $pH_{rbc,S} = 0.795pH_{pl,S} + 1.357$	7.24	Unitless
$[DPG]_{rbc,S}$	Standard 2,3-DPG concentration in RBCs	4.65×10^{-3}	M
T_S	Standard temperature of blood	37	°C
pH_{rbc}	pH in RBCs, related to plasma pH by: $pH_{rbc} = 0.795pH_{pl} + 1.357$)	Variable	Unitless
R_{rbc}	Gibbs-Donnan ratio for electrochemical equilibrium of protons or bicarbonate ions across the RBC membrane ($R_{rbc} = [H^+]_{pl}/[H^+]_{rbc} = [HCO_3^-]_{rbc}/[HCO_3^-]_{pl}$; $R_{rbc} = 10^{-(pH_{pl}-pH_{rbc})} = 10^{-(0.205\cdot pH_{pl}-1.357)}$)	Variable (0.692 at pH_{pl} = 7.4)	Unitless
$a_{O2,S}$	Solubility of O_2 in water at standard temperature (37 °C)	1.46×10^{-6}	M/mmHg
$a_{CO2,S}$	Solubility of CO_2 in water at standard temperature (37 °C)	3.27×10^{-5}	M/mmHg
Hct_S	Standard hematocrit (volume fraction of RBCs in blood)	0.45	Unitless
$[Hb]_{bl,S}$	Standard hemoglobin concentration in blood	2.33×10^{-3}	M
$[Hb]_{rbc,S}$	Standard hemoglobin concentration in RBCs ($[Hb]_{rbc}=[Hb]_{bl}/Hct$)	5.18×10^{-3}	M
W_{pl}	Fractional water space of plasma	0.94	Unitless
W_{rbc}	Fractional water space of RBCs	0.65	Unitless
W_{bl}	Fractional water space of blood: $W_{bl} = (1-Hct)\cdot W_{pl} + Hct\cdot W_{rbc}$	0.81	Unitless
$[O_2]_{tot}$	Total O_2 concentration of whole blood: $[O_2]_{tot} = W_{bl}\cdot a_{O2}\cdot P_{O2} + 4\cdot Hct\cdot[Hb]_{rbc}\cdot S_{HbO2}$	Variable	M
$[CO_2]_{tot}$	Total CO_2 concentration of whole blood: $[CO_2]_{tot} = W_{bl}\cdot a_{CO2}\cdot P_{CO2} + ((1-Hct)W_{pl}+Hct\cdot W_{rbc}\cdot R_{rbc})(K_1\cdot a_{CO2}\cdot P_{CO2}/[H^+]_{pl}) + 4\cdot Hct\cdot[Hb]_{rbc}\cdot S_{HbCO2}$ (parameter K_1 defined above)	Variable	M

[#]Estimated based on model fittings to the data of Bauer and Schröder (1972) at T = 37 °C (see Fig. 3E)

[*]Estimated based on model fittings to the data of Matthew et al. (1977) at T = 30 °C (see Fig. 3F)

[$]Estimated based on model fittings to the data of Severinghaus and colleagues (Roughton *et al.*, 1972; Roughton & Severinghaus, 1973; Severinghaus, 1979) in normal human blood at standard physiological conditions